Mesoscopic structures in ferroelastic crystals: needle twins and right-angled domains



1996 J. Phys.: Condens. Matter 8 8477

(http://iopscience.iop.org/0953-8984/8/44/004)

J. Phys.: Condens. Matter **8** (1996) 8477–8495. Printed in the UK

# Mesoscopic structures in ferroelastic crystals: needle twins and right-angled domains

E K H Salje† and Y Ishibashi‡

† Department of Earth Sciences and Interdisciplinary Research Centre, University of Cambridge, Downing Street, Cambridge CB2 3EQ, UK

‡ Department of Applied Physics, School of Engineering, Nagoya University, Chikusa-ku, Nagoya 464-01, Japan

Received 10 May 1996, in final form 17 July 1996

**Abstract.** The shape and orientation of twin walls are calculated within the limits of elasticity theory. Single twin walls are oriented along lattice planes which are determined by the condition that the variation in the spontaneous strain through the twin walls does not generate secondary strain fields. The twin walls have a finite thickness which is described by the Landau–Ginzburg theory. Two twin walls can bend towards each other and form a wedge-shaped junction. The trajectories of the twin walls in the plane perpendicular to the junction are needle shaped so that domains enclosed by the twin walls are commonly called 'needle domains'. It is shown that the actual shape of the trajectory varies widely between straight lines (i.e. planar walls near the junction) to parabolic or exponential (i.e. curved twin walls near the junction which make the needle tip appear blunt). The essential physical parameters which determine the shape of the trajectory are, firstly, the energies to bend a wall segment, secondly, the energy required to rotate a planar wall segment in an elastically anisotropic medium and, thirdly, the Peierls energy which is required to move a walls segment laterally. Various characteristic trajectories are discussed including those of junctions between orthogonal walls.

## 1. Introduction

Ferroelastic domain structures are one of the most common non-equilibrium features in materials and minerals and, indeed, virtually all ferroelastic or co-elastic materials show the formation of characteristic microstructures when they undergo a structural phase transition [1]. Single-domain crystals can be produced under specific conditions but, for example, it requires great experimental skill to eliminate twin walls under the application of uniaxial stress in rather pure materials [2–4].

It is a common observation that ferroelastic framework structures undergo (nearly) continuous phase transitions [1]. The microstructures in such materials have nothing to do with nucleation-and-growth mechanisms during the phase transition but may originate from lattice imperfections, the effects of the surface and frozen-in fluctuations. The general thermodynamic description of 'twinning' and 'tweeding' as the most common microstructures is rather well understood [5–22]. What are much less understood are the finer details of the twin structures on a mesoscopic scale. This fine structure involves the formation of needle domains and wall junctions, and the evolution of wall profiles when they approach the surface of the crystal, etc [1].

The reasons for our ignorance in this field are twofold. Firstly, the mesoscopic length scale between 50 and 200 Å is experimentally difficult to access. The observation by electron

0953-8984/96/448477+19$19.50  

microscopy requires the simultaneous analysis of a strain pattern related to twin walls and the high-resolution imaging of the internal structure of such walls. Such simultaneous observations are clearly a difficult task for the experimentalist. The situation has somewhat improved with the advent of high-resolution x-ray diffraction facilities which allow the direct and convenient observation of the diffuse diffraction around Bragg reflections [23]. The diffuse diffraction profiles can in many cases be directly correlated with the mesoscopic domain structures, e.g. the thickness of a twin wall was determined in this way. In fact, this technique is sensitive enough to 'see' very few walls indeed; wall patterns with one wall every 10 000 Å have been measured [24–27].

The second reason for the lack of knowledge in this field is the somewhat esoteric nature of the subject. Although mathematically appealing, it seemingly lacks the potential for application of a technical nature. This assessment is not correct, however. With the advent of high-temperature superconductors it became immediately clear that their current characteristics are related to the mesoscopic structure. In the field of semiconducting thin films and devices, the tendency to miniaturize to a true nanostructure will presumably lead to the use of ferroelastic materials as convenient templates with the appropriate microstructure. Nonlinear optics makes use of twin patterns as waveguides and dielectric relaxor materials are based on the fact that certain ferroelectric materials always show intrinsic microstructures. Finally, in the general area of geosciences, the analysis of mesoscopic structures has for several years been used for the determination of past geological events [28–35].

What is lacking at this stage of the development is a detailed study which allows the quantitative description of the wall profiles and understanding of the underlying physical features which determine wall profiles. In this paper we focus on the bending of domain walls which leads to the formation of needle domains, the pinning by isolated point defects and the bending of walls near 90° junctions. We also derive some simple dynamical features of twin walls.

The paper is organized as follows. First the energy expressions for wall rotations and wall bending are reviewed. In section 3 the wall trajectories are derived for some specific physical situations. In section 4 the dynamical and kinetic properties of wall movements are anticipated; experimental observations will be compared with the results of this theoretical treatment in a forthcoming paper.

## 2. The elastic strain interaction

The internal structure of twin walls is largely determined by the short-range interaction between atoms and the way that the atomic coordinates and occupancies reflect the spatial variations in the thermodynamic order parameter of the ferroelastic or co-elastic phase transition. In such materials, the structural variations lead to elastic relaxations of the crystal structure, producing long-range strain fields. The strain fields generated by mesoscopic structures need not lead to a macroscopic deformation of the sample or a variation in the average lattice parameters. The latter would be expressed by the macroscopic spontaneous strain of the sample and it is usually observed that different mesoscopic structures (e.g. single crystals or heavily twinned materials) show almost the same macroscopic lattice parameters and, thus, the same spontaneous strain. Local strain fields reflect simply the pulling and pushing of atoms due to the formation of mesoscopic structures whereby the restoring forces obey Hooke's law with appropriate elastic constants. Such strain fields exist not only in displacive phase transitions but also in those of the order–disorder type. When atomic ordering takes place in one part of the crystal it inevitably pulls and pushes

neighbouring atomes and/or structural units, i.e. it creates a local displacement field. This field then displaces atoms beyond it and hence propagates elastically to distant parts of the crystal via a knock-on effect. The experimental observation of domain boundaries, such as twin walls, shows that their strain profiles corresponds well to that predicted from classic theory of elastic interactions, ignoring any additional short-range interactions.

Let us first consider twinning due to a phase transition with one non-degenerate order parameter $Q$ and the spontaneous strain $e_i$. Starting from the Landau–Ginzburg potential of such a phase transition, one finds for bilinear coupling between $Q$ and $e_i$

$$G = \tfrac{1}{2}A(T - T_c)Q^2 + \tfrac{1}{4}BQ^4 + \lambda_i e_i Q + \tfrac{1}{2}C_{ik}e_i e_k + \tfrac{1}{2}g(\nabla Q)^2 \tag{1}$$

where summation takes place over all repeated indices. If the system can relax elastically, the equilibrium condition becomes

$$\delta G/\delta e_i = 0 \tag{2a}$$

or

$$\lambda_i Q + C_{ik}e_k + C_{ii}e_i = 0 \qquad i \neq k. \tag{2b}$$

This equation shows that all strain components are proportional to the order parameter $Q$ as required in proper ferroelastic phase transitions. We can then rewrite the Gibbs free energy as a function of the strain only and focus on the symmetry-breaking strain which generates the mesoscopic structure. We call this strain $e$; its macroscopic equivalent is $e_{spontaneous}$. The Gibbs free energy is

$$G = \tfrac{1}{2}C(T)e^2 + \tfrac{1}{4}C'e^4 + \tfrac{1}{2}g(\nabla e)^2. \tag{3}$$

The profile of a twin wall follows from the condition that the total strain energy of the wall is minimal:

$$\int G(e, \nabla e)\,\mathrm{d}y = \text{minimum} \tag{4}$$

where $y$ is the coordinate along the normal to the part of the twin wall under consideration. The solution of the minimum condition is given by the Euler–Lagrange equation of $G$:

$$(\partial/\partial y)[\partial G/\partial(\nabla e)] = \partial G/\partial e. \tag{5}$$

When replacing $G$ by its full expression, one finds that

$$g\,\mathrm{d}^2e/\mathrm{d}y^2 = Ce + C'e^3. \tag{6}$$

The solution of this differential equation was reviewed in great detail in [1]. The strain profile of a twin wall is

$$e = e_0 \tanh(y/w) \tag{7}$$

where $e_0 = (C/C')^{1/2}$ is the spontaneous strain in the uniform part of the sample and $w = \frac{1}{2}(g/C)^{1/2}$ is a measure of the thickness of the twin wall.

Experimentally, such twin wall profiles were observed in feldspars, high-temperature superconductors and ferroelastic lead phosphate [24, 25, 36–41]. Twin walls in this approximation are planar as long as there is no interaction with other twin walls, impurities or the crystal surface. A most common interaction originates from a configuration of four domain walls where two pairs form corners as depicted in figure 1. The corner junctions attract each other with a force

$$F = Ar\ln(R/r)$$

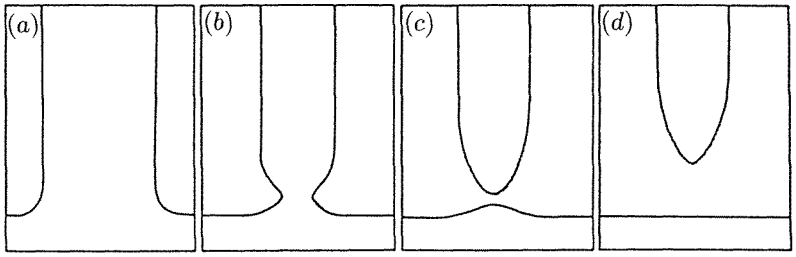


**Figure 1.** Formation of needle twins. (*a*) Two right-angled domain walls separating two domains are too far apart to interact. (*b*) Another pair of domains are sufficiently close for mutual attraction to occur. (*c*) With a sufficiently fast cooling rate, this activated state can be overcome. (*d*) The resulting needle twin migrates farther into the surrounding domain under the influence of the strain field between its tip and the new planar boundary.

where $r$ is the distance between the two junctions and $R$ is the unbinding distance. For sufficiently short starting distances between the junctions, the junctions will move towards each other and join. Once the two junctions have joined to form a single junction, a needle domain is formed. The new junction is the tip of the needle (figure 1). The needle can then retract, which is a very common annealing mechanism for twin structures (see [1] for detailed discussions and examples).

We now focus on the discussion of the shape of the needle domain as shown in figure 2. At regions far away from the needle tip, the planar wall is maintained by local pinning forces. These pinning forces disallow the lateral movement of the wall along the $y$ direction. At the tip, the bending force $F$ pulls the wall. The same situation is encountered if the force $F$ relates to point defects or surface effects; the following treatment applies for all these cases. What matters is that a force is exerted at a well defined position of the wall and that the part of the wall far away from this position maintains its original shape. The actual shape of the wall is considered to be uniform along the $z$ direction; the bending takes place in the $x$–$y$ plane. The wall profile is given as its trajectory in the $x$–$y$ plane. We now discuss the relevant forces and energies which are opposed to the bending of the wall. Local theories are used throughout this paper because non-local corrections are expected to be small for geometric configurations as encountered in needle domains, etc. Possible dislocations, etc, at the junction are not considered here because they have little effect on the overall shape of the wall trajectories.

### *2.1. The elastic anisotropy energy*

The strain field changes its sign in the middle of the twin wall. One twin domain has a positive spontaneous strain; the other has a negative spontaneous strain. Any such strain is described uniquely by an atomic displacement field $u(r)$ which has in a three-dimensional crystal three components. The strain tensor has six components so that it is clear that some correlation must exist between the various strain components for an arbitrary displacement field. These correlations are ensured by the compatibility condition which requires that inhomogeneous strains do not destroy the continuity of the crystal structure. In other words, we disallow the formation of cracks when the domain walls bend. Mathematically, continuity is elegantly described by the condition that the second

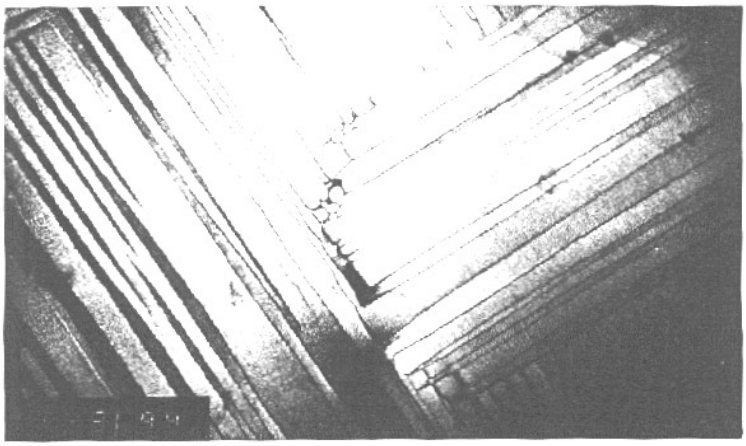

**Figure 2.** Characteristic microstructure of orthorhombic $YBa_2Cu_3O_7$ showing needle domains at various stages of their development. In the centre, two domains are still attached to an orthogonal wall. The needle tip is almost formed. Arrays of needle domains (so-called domain combs) are seen at the top and bottom right-hand side. Stranded needles without an orthogonal wall are seen at the left-hand side of the image. (Length scale of black stripe, 0.1 $\mu$m.)

derivatives of the displacement field are independent of the order in which the derivatives are taken [16]:

$$\delta^2 u_i/(\delta x_j \delta x_k) = \delta^2 u_i/(\delta x_k \delta x_j) \tag{8}$$

i.e. no singularity of the displacement field exist at any point in space. In a two-dimensional $x'$–$y'$ plane, the compatibility relation can easily be rewritten in terms of the strain components only:

$$(\delta^2/\delta x'^2)e_{y'y'} + (\delta^2/\delta y'^2)e_{x'x'} = 2(\delta^2/\delta x'\,\mathrm{d}y')e_{x'y'}. \tag{9}$$

In terms of the symmetry-adapted strains

$$e_{hom} = e_{x'x'} + e_{y'y'} \tag{10}$$

$$e_{x^2-y^2} = e_{x'x'} - e_{y'y'} \tag{11}$$

$$e_{xy} = e_{x'y'} \tag{12}$$

these conditions can be further simplified. The homogeneous strain $e_{hom}$ stretches the plane as a whole, whereas the two shear strains act along the $\langle 10\rangle$ and $\langle 11\rangle$ directions respectively. Converting the strain into reciprocal space by Fourier transformation we find the simplest form of the compatibility relation:

$$e_{hom}(k) = e_{x^2-y^2}(k)\cos(2\alpha) + e_{xy}(k)\sin(2\alpha) \tag{13}$$

where $\alpha$ is the angle measured from the positive $k_x$ axis. This equation leads to the following important conclusion [16]. Let the spontaneous strain of the phase transition be $e_{x^2-y^2}$. This strain can then exist on its own for any wavevector $k$ for an angle $\alpha = 45^\circ + n90^\circ$. This means that a wall profile of the $x^2 - y^2$ type can be formed for the crystallographic $\langle 110\rangle$ directions but not along any other direction. This preferred orientation of the twin wall is often called the 'elastically soft direction' because the formation of twin walls in this direction requires the minimum excess energy. If a wall is locally bending away from the

soft direction it will automatically generate strain fields with symmetries which are different from that of the spontaneous strain. If we constrain the size of the crystal ($e_{hom} = 0$), we find that a bending of a wall with $e_{x^2-y^2}$ symmetry will generate strain of the $e_{xy}$ symmetry:

$$e_{xy} = -e_{x^2-y^2}\cos(2\alpha). \tag{14}$$

As the strain energy increases with increasing square of the strain component, we find that bending leads to an increase in the wall energy (for small bending angles) proportional to the square of the bending angle. For small $k$ vectors (i.e. long-wavelength modulations) the excess energy due to the compatibility condition is the elastic anisotropy energy:

$$E_{anisotropy}(\delta\alpha) = \tfrac{1}{2}V[C_2 + C_1\sin^2(2\,\delta\alpha)\,e^2_{x^2-y^2} + [C_3 + C_1\cos^2(2\,\delta\alpha)]\,e^2_{xy}(k) \\ -C_1\sin(4\,\delta\alpha)\,e_{x^2-y^2}(k)\,e^*_{xy}(k) \tag{15}$$

where $C_i$ indicates combinations of the relevant elastic constants. The angular dependence of the anisotropy energy for a wall segment can be expressed as

$$E_{anisotropy}(\delta\alpha) = \tfrac{1}{2}U\sin^2(2\,\delta\alpha) \tag{16}$$

where $U$ is a combination of elastic constants and the relevant Fourier components of the strain field in the wall. This angle-dependent wall energy is universal for all elastic systems and does not depend on any underlying atomistic model. The only material parameter in the problem is $U$ which describes the stiffness of the system with respect to any misorientation of a straight domain wall. For small angles $\alpha$ and small curvatures, the angle can be equated with the local slope of the wall in the $x$–$y$ plane:

$$\delta\alpha = -\mathrm{d}y/\mathrm{d}x. \tag{17}$$

For small angles the anisotropy energy is simply a quadratic function of the slope of the wall in the $x$–$y$ plane.

$$E_{anisotropy} = U(\mathrm{d}y/\mathrm{d}x)^2. \tag{18}$$

Equations (16) and (18) will be used in the following for the calculation of wall trajectories.

### *2.2. The bending energy*

While $E_{anisotropy}$ describes the excess energy of a straight part of a wall for orientations which are not along the elastically soft directions, the wall bending energy describes the excess energy needed to introduce curvature in the wall trajectory. Experimental evidence from x-ray diffraction studies and some observations using transmission electron microscopy show that the characteristic wall thickness $w$ is of the order of a few lattice repetition lengths. In the case of framework structures with large crystallographic unit cells, the wall thickness is some 20 Å. If such a wall is curved, the atomic distances in the wall are stretched on one side of the wall and compressed on the other side of the wall. The neutral layer is in the middle where there is no extension or compression. The cross section along the $y$ axis increases in the bend region by

$$\delta y_{bend} = [(R + x)/R]\delta y_{unbend} = (1 + x/R)\delta y_{unbend} \tag{19}$$

where $R$ is the bending radius. Each element $\delta y$ is hence extended with the component of the strain tensor given by

$$u_{xx} = x/R. \tag{20}$$

The elastic response due to the strain is described by the stress tensor with

$$\sigma_{yy} = Ex/R \tag{21}$$

where $E$ is the stiffness parameter equivalent to Young's modulus in elastic theory [42]. The bending energy is proportional to $u_{xx}\sigma_{yy}$, i.e. it depends on $R$ as $1/R^2$ which, in turn, is proportional to the bending angle $\delta\Phi$:

$$E_{bending} = \int \tfrac{1}{2} I E (\delta\Phi)^2 \, \mathrm{d}l \tag{22}$$

where $I$ is the momentum of inertia and $\mathrm{d}l$ is the length element along the wall trajectory in the $x$–$y$ plane. We now define the angular momentum of the bend as

$$M = I E \, \delta\phi \tag{23}$$

in analogy to the mechanical bending of macroscopic elastic bodies. The bending energy becomes then

$$E_{bending} = \int \frac{M^2}{2 I E} \, \mathrm{d}l. \tag{24}$$

In order to characterize the bending we put a tangential reference plane at any point of the wall. Its intersection with the $x$–$y$ plane defines the tangential vector $\boldsymbol{t}$. The bending angle for a length element $\mathrm{d}l$ is

$$\delta\phi = \boldsymbol{t} \times \frac{\mathbf{d}\boldsymbol{t}}{\mathrm{d}l}. \tag{25}$$

For small angles the vector $\boldsymbol{t}$ is along the direction of the unbent wall in the pinned area with $t = x$. The orientation of $\boldsymbol{t}$ in the bent region is given by the slope of the trajectory $\boldsymbol{t} = \mathbf{d}\boldsymbol{y}/\mathrm{d}l$ with

$$\mathrm{d}t/\mathrm{d}l = \mathrm{d}^2y/\mathrm{d}l^2 = \mathrm{d}^2y/\mathrm{d}x^2. \tag{26}$$

The energy of the wall bending can then be written as

$$E_{bending} = \tfrac{1}{2} I E \int \left(\frac{\mathrm{d}^2y}{\mathrm{d}x^2}\right)^2 \mathrm{d}x. \tag{27}$$

The bending energy per length element of the wall

$$E_{bending} = \tfrac{1}{2} I E (\mathrm{d}^2y/\mathrm{d}x^2)^2 = S(\mathrm{d}^2y/\mathrm{d}x^2)^2 \tag{28}$$

is quadratic in the second derivatives of the spatial coordinates. This is in contrast with $E_{anisotropy}$ which depends on the square of the first derivatives of the wall trajectories. Both energies are positive, i.e. they increase with increasing deviation from the ideal wall orientation. Before we can discuss the actual wall profiles, we first derive the equilibrium condition for a bent wall. Let a force act on one point of the wall trajectory, say at the tip of the needle. This force is then compensated by all forces inside the cross section of the wall. If the external force is applied at points, then the compensation forces are uniform everywhere between these points. We denote the equivalent stress in the walls as $-\sigma_{internal}\boldsymbol{f}$ where $\boldsymbol{f}$ is the unit vector along $\boldsymbol{F}$. The angular momentum for each length element $\mathbf{d}\boldsymbol{l}$ is

$$\mathbf{d}\boldsymbol{M} = -\mathbf{d}\boldsymbol{l} \times (-\sigma_{internal}\boldsymbol{f}) \tag{29}$$

or, with the tangential vector $\boldsymbol{t} = \mathbf{d}\boldsymbol{l}/\mathrm{d}l$ as unit vector,

$$\mathbf{d}\boldsymbol{M}/\mathrm{d}l = (-\sigma_{internal}\boldsymbol{f}) \times \boldsymbol{t}. \tag{30}$$

For uniform external forces, the stress field is a linear function of the length of the wall. In order to find the angular momentum for constant values of $\mathrm{d}\boldsymbol{\sigma}_{internal}/\mathrm{d}l = \boldsymbol{K}$ we differentiate the last equation and find

$$\mathrm{d}^2\boldsymbol{M}/\mathrm{d}l^2 = \boldsymbol{t} \times (\mathrm{d}\sigma_{internal}/\mathrm{d}l\,\boldsymbol{f}) = \boldsymbol{t} \times \boldsymbol{K}. \tag{31}$$

We finally express the angular momentum in terms of the spatial derivatives and find the characteristic bi-quadratic equation of elasticity theory of walls:

$$I E \, \mathrm{d}^4 y/\mathrm{d}x^4 = K_y \tag{32}$$

where $K_y$ is the $y$ component of the vector $\boldsymbol{K}$. This equation determines the curvature of a twin wall or any other object (e.g. an antiphase boundary) in the case of uniform applied forces.

## 3. Wall trajectories for specific physical situations

### *3.1. Curvature-dominated trajectories*

*3.1.1. Strained domain walls with one pinning centre.* A rather common physical situation for wall bending in materials with pinning centres is shown in figure 3. A macroscopic sample is sheared so that domain 1 is stabilized with respect to domain 2. The wall moves in order to increase the size of domain 1 under a constant force per unit wall surface element applied to the wall (i.e. $K =$ constant). When the wall hits a defect, a point force is superimposed on the uniform force field and the wall bends around the defect. For thick walls in rather isotropic media, the wall profile is determined by the bending energy with $\mathrm{d}^4 y/\mathrm{d}x^4 = 0$ everywhere except at the locus of the point force (e.g. $x = h/2$):

$$\mathrm{d}^4 y/\mathrm{d}x^4 = K\delta(x - h/2). \tag{33}$$

The surface of the crystal is allowed to relax so that the boundary conditions are $y = 0$ at $x = 0$ and $x = h$. The solution of the differential equation is a polynomial of third order which is symmetrical with respect to $x = h/2$. No second-order terms exist because of the condition that the wall is flat ($y'' = 0$) without applied force. The required solution is

$$y = (1/h^3) y_{max} x(3h^2 - 4x^2) \qquad \text{for } x < h/2 \tag{34}$$

$$y = (1/h^3) y_{max} (h - x)(-h^2 + 8xh - 4x^2) \qquad \text{for } x > h/2 \tag{35}$$

where $y_{max} = Kh^3/48$ is the maximum deviation of the wall centre from the surface. Around the defect the wall is parabolically bent with a straighter shape farther away from the pinning centre. As there is no elastic anisotropy energy present in this example, the wall is never planar along the elastically soft direction but is bent throughout the entire crystal.

*3.1.2. Two pinning centres at the surface of the crystal.* In this case, the point forces are at each end of the wall whereas the rest of the wall is subject to a constant dragging force due to the macroscopic shear of the sample. The differential equation which describes the wall trajectory is now

$$\mathrm{d}^4 y/\mathrm{d}x^4 = K[\delta(x) + \delta(x - h)] \tag{36}$$

with solution

$$y = (K/24) x(x^3 - 2hx^2 + h^3) \tag{37}$$

where $h$ is again the thickness of the sample in the $x$ direction. The total wall profile is almost identical with that in section 3.1.1. The fundamental difference is how the wall reacts to the pinning centre. In the case of the pinning centre in the middle of the crystal, we find that the wall bends around the centre with a parabolic curvature. In the case of surface pinning, the wall simply rotates near the centres but does not curve. The maximum curvature is again in the middle of the crystal because the two rotated parts of the wall have to connect in a smooth manner. The important conclusion from the comparison of the

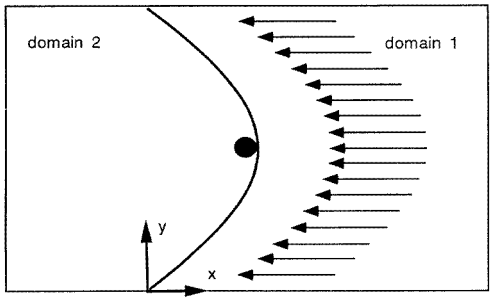


**Figure 3.** Uniform drag on the wall with one pinning centre; the wall profile is bending dominated.

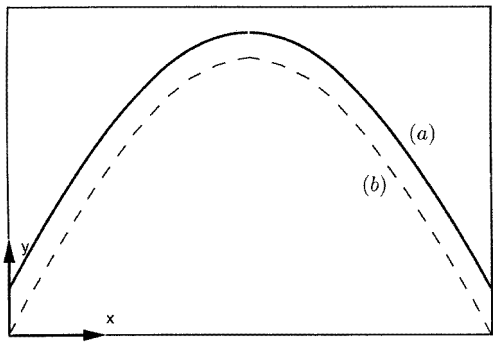


**Figure 4.** Comparison of two wall profiles with a pinning centre (curve a) and surface pinning (curve b).

shapes in figure 4 is that it is impossible to distinguish between the possible origins of a bent contour from the experimental observation alone; the contour may be due to one defect in the middle of the bend or several defects at the outside.

*3.1.3. Elastic drag with one pinning centre.* The wall is again moved by external forces and hits a local defect. In contrast with the case discussed in section 3.1.1 the wall is allowed to relax along the $y$ direction at great distance from the pinning centre. Such relaxation is achieved by a macroscopic deformation of the sample. The restoring force of the relaxation is elastic in nature and increases linearly with the wall displacement $K = Py$. The trajectory is described by

$$S\,\mathrm{d}^4y/\mathrm{d}x^4 = -PyK'\delta(x). \tag{38}$$

For an infinite crystal, the boundary conditions are $y = 0$ at $x = \infty$ and $x = -\infty$, the bending must be continuous at $y = 0$ in $y, y'$ and $y''$. The solution of the differential equation is

$$y = y_{max}\exp(-\beta|x|)[\cos(\beta|x|) + \sin(\beta|x|)] \tag{39}$$

with the characteristic length

$$\lambda = 1/\beta = (4S/P)^{1/4}. \tag{40}$$

The new aspect of this solution, in contrast with the case discussed before, is that there is an intrinsic length scale of the problem which allows the wall to bend back to the original orientation of the unperturbed crystal. This solution will always apply if there are atomic Peierls forces which determine the orientation of the wall so that a free rotation of the wall becomes energetically too costly. As a consequence the original contour of the wall at large distances from the pinning centre is restored. This physical situation is expected in most materials besides very pure samples with no Peierls forces which were discussed before. The trajectory of the wall with Peierls forces is shown in figure 5; the bending of the wall is strongest around the pinning centre and decays exponentially with increasing distance from the centre.

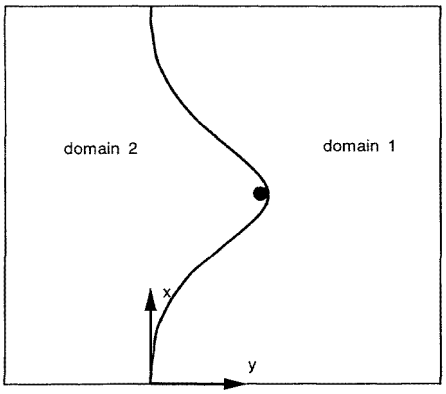


**Figure 5.** Wall bending near a pinning centre with dominant bending energy and elastic lattice relaxation.

*3.1.4. Needle domain without relaxation.* We now consider a needle domain which is rigidly pinned outside the region of the tip of the needle and its curvature is determined by the bending forces alone. The position of the tip is at $x = 0$. At this point the force which generated the tip is applied. No further forces are considered:

$$d^4y/dx^4 = K\delta(x) \tag{41}$$

with the solution

$$y = (y_{max}/2\lambda^3)(\lambda - x)^2(2\lambda + x) \qquad \text{for } x < \lambda \tag{42}$$

where $y_{max}$ is the maximum deviation of the wall trajectory from the original wall and $\lambda$ is the length of the needle tip, i.e. the length of the area which is unpinned. The length scale is now determined by the unpinning behaviour. It is not an intrinsic length scale of the problem although one might expect that this length is correlated with the value of $y_{max}$. The shape of the wall trajectory is shown in figure 6. Note that the wall is rather smoothly bent with no singularity at the point of unpinning at $x = \lambda$.

### *3.2. Anisotropic wall energies*

*3.2.1. Needle domains for weak bending.* We first consider Peierls forces which are a linear function of the wall displacement $y$ and simplify the anisotropy energy for small angles to

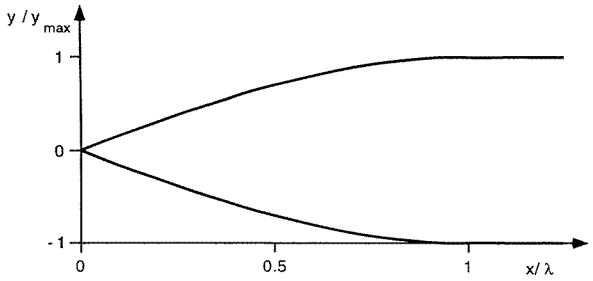


**Figure 6.** Wall profile for needle domain with a large curvature energy and no lattice relaxation.

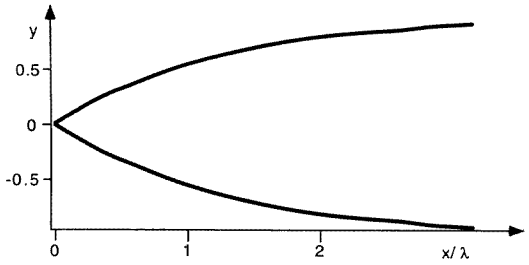


**Figure 7.** Profile of an anisotropy-dominated needle with lattice relaxation.

include only the quadratic term in the energy density

$$E = U(\mathrm{d}y/\mathrm{d}x)^2 + Py^2. \tag{43}$$

The wall trajectory is then determined by the Euler–Lagrange equation with

$$-2Py + 2U\,\mathrm{d}^2y/\mathrm{d}x^2 = 0. \tag{44}$$

The solution is an exponential decay with

$$y = y_{max}\exp(-x/\lambda) \tag{45}$$

where $y_{max}$ is again the maximum deviation from the unperturbed wall at the needle tip. The length scale $\lambda$ is given by

$$\lambda = (U/P)^{1/2} \tag{46}$$

and is an intrinsic property of this wall contour. It is determined by the ratio of the anisotropy energy to the Peierls energy. For large pinning forces the needle tip is short, whereas for small pinning forces the tip becomes long and narrow. The profile is smooth and shows a maximum bend near the shaft of the tip (figure 7). At the tip itself the trajectory is linear.

*3.2.2. Unpinning of the needle tip.* We now discuss a case similar to that described in section 3.1.4. The pinning is strong inside the original wall whereas the bent part of the wall is totally unpinned. A typical physical situation can be described as follows. Let the pinning be generated by impurity atoms. Such impurities often cluster on the walls. This effect is called 'decoration' of a twin wall. If a decorated wall moves, the impurity atom cannot follow quickly enough and the pinning effect is lost. Abrupt depinning in strong electric fields is commonly observed in ferroelectric crystals. If only part of the wall moves

owing to the formation of a needle domain, this part is unpinned while the remainder of the wall remains pinned. Corrections of the kind discussed in section 3.2.1 are needed to describe the region where the unpinning starts near the shaft of the needle tip. For the actual tip, the trajectory is described by $P = 0$ with the boundary condition $y = 0$ at $x > \lambda$. With

$$2U\,\mathrm{d}^2y/\mathrm{d}x^2 = 0 \tag{47}$$

the solution becomes

$$y = y_{max}(1 - x/\lambda) \qquad \text{for } x < \lambda. \tag{48}$$

The trajectory is linear over large areas of the needle with exponential corrections near the shaft of the needle tip. The wall profile is shown in figure 8.

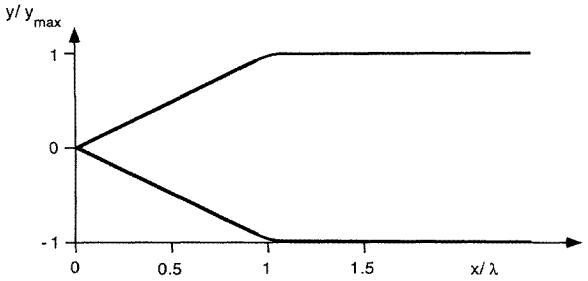


**Figure 8.** Linear needle tip for strong anisotropy energies and no lattice relaxation.

*3.2.3. Nonlinear Peierls forces.* The wall is again strongly pinned in its unperturbed region. Instead of letting the pinning force disappear completely close to the needle tip we consider now the case when the Peierls force decays slowly with the bending of the wall. The Peierls potential is now not parabolic but is flatter than the parabolic potential for larger values of $y$. An appropriate energy density is

$$E = U(\mathrm{d}y/\mathrm{d}x)^2 + P[1 - \cos(y/y_0)]. \tag{49}$$

The Euler–Lagrange equation for this Peierls potential is

$$U(\mathrm{d}^2y/\mathrm{d}x^2) - P\sin(y/y_0) = 0 \tag{50}$$

which can be integrated directly with

$$x = \int \left(\frac{E_0}{U} - \frac{P}{U}\cos\left(\frac{y}{y_0}\right)\right]^{-1/2} \mathrm{d}y \tag{51}$$

where $E_0$ is the total energy of the configuration. The integral can be expressed in terms of elliptical functions. For small values of $y/y_0$ the cos function can be expanded so that the trajectory is determined by

$$x = \int \left[\left(\frac{E}{U} - \frac{P}{U}\right) + \frac{Py^2}{2Uy_0^2}\right]^{-1/2} \mathrm{d}y. \tag{52}$$

We now distinguish between two cases depending on the magnitude of the Peierls contribution compared with the wall energy.

(a) For small Peierls forces ($E_0 \gg P$), the wall profile becomes approximately exponential with a characteristic length of $(2U/P)^{1/2}$ near the shaft of the needle while the profile at the tip of the needle is linear. The inverse function of the trajectory is

$$x = x_0 + (2U/P)^{1/2} \ln\{y + y^2 + 2(E/P - 1))^{1/2}\}. \tag{53}$$

This trajectory is plotted in figure 9.

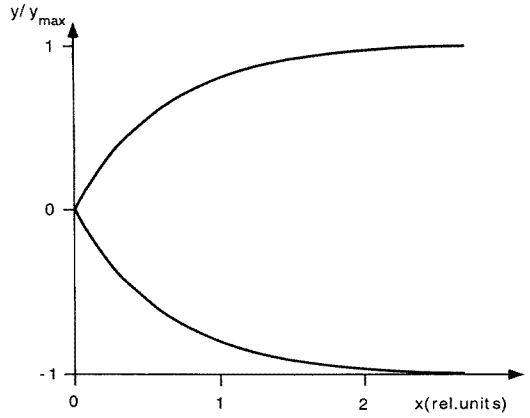


**Figure 9.** Periodic Peierls force with strong anisotropy energy.

(b) For strong Peierls forces $E_0 = P$ the trajectory is parabolic with the centre of the parabola at the shaft of the needle to ensure an optimal fit between the planar part of the twin wall and the needle tip. The trajectory is shown in figure 10.

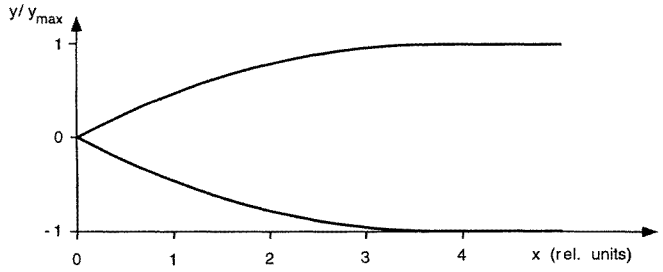


**Figure 10.** Needle domain with strong Peierls forces and high anisotropy energy.

Other forms of the Peierls potential can be envisaged. Their general effect is that any reduction in Peierls forces with increasing bending of the needle (i.e. with increasing values of $y$) will lead to blunter needle tips with stronger curvature of the wall trajectory near the tip of the needle. At the shaft of the needle the trajectory of the needle tip will merge with the unperturbed wall asymptotically. For strong linear Peierls forces the trajectory is parabolic at the shaft.

### *3.3. Mixing of length scales for the elastic anisotropy energy and the bending energy*

Characteristic length scales have resulted so far from the simultaneous occurrence of Peierls energies and either the elastic anisotropy energy or the bending energy. In each case, the length scale was determined by the ratio of the energy coefficients with the power 1/2 or 1/4. A similar length scale appears when the two anisotropy energies and the bending energies apply simultaneously together with the Peierls energy. The energy density is

$$E = Py^2 + U(\mathrm{d}y/\mathrm{d}x)^2 + S(\mathrm{d}^2y/\mathrm{d}x^2)^2. \tag{54}$$

The Euler–Lagrange equation for this case is

$$-Py + U\,\mathrm{d}^2y/\mathrm{d}x^2 - S\,\mathrm{d}^4y/\mathrm{d}x^4 = 0. \tag{55}$$

Fourier transformation leads to the equivalent equation for each Fourier component $y_k$:

$$Py_k + Uk^2y_k + Sk^4y_k = 0 \tag{56}$$

with

$$k^2 = -U/(2S) + -\{(U/2S)^2 - P/S\}^{1/2}. \tag{57}$$

For sufficiently small values of $P$, solutions are found with purely imaginary values of $k$. They represent an exponential decay of the trajectory for each Fourier component with the characteristic $k$ vector given by

$$k^2 = -P \tag{58a}$$

and

$$k^2 = -U/S + P < 0. \tag{58b}$$

The length scales are given by $P^{-1/2}$ and $(U/S - P)^{-1/2}$, respectively.

### *3.4. 'Right-angle' twin walls*

As shown above in section 2.1 the compatibility relation has always two solutions with walls which have orthogonal normal vectors with respect to the coordinate system of the paraelastic phase. In some cases these walls may be $W$ and $W'$ walls which can intersect and form corners. It is customary to call these corner configurations 'right-angled' domains. This term is somewhat misleading, however, because the angle between the two walls is not exactly $\pi/2$ but either $\pi/2 + \omega$ or $\pi/2 - \omega$, where $\omega$ is the value of the spontaneous strain of the sample [1]. In materials with a small spontaneous strain (some $10^{-3}$, say) the deviation of the angle from $\pi/2$ is too small to be seen in electron microscopy or optical images while for most ferroelastics with spontaneous strains of some 2% such deviations are clearly recognized. It was shown that this misfit of the wall angle from $\pi/2$ is essential for the understanding of the shape of the corner tip. Elastic strain energies of the bulk may lead to a rounding of the corner or may make the corner bulge out. Using our present approach we also predict rounded corners for a different reason. In order to derive the trajectory we define a coordinate system which is rotated by $-\pi/4$ and ignore the deviation of the corner angle from $\pi/2$. The configuration is shown in figure 11. The straight part of the wall is at an angle $\alpha = -\pi/4$ and $\alpha = +\pi/4$ (i.e. $\mathrm{d}y/\mathrm{d}x = 1$ and $-1$, respectively). The role of the Peierls forces is taken into account by the boundary condition that the walls at large values of $x$ have to be asymptotically close to the original straight wall. The wall energy is formulated as the sum of the anisotropy energy and the bending energy. In the case of the anisotropy energy, the effect of contracting the length element $\mathrm{d}l$ in the bend of the wall has to be considered. A similar argument is not necessarily valid for the bending energy

because the bending may thicken the wall in the bend and thereby increase the bending force. Using the projection of the length element on the axis we find the energy expression which has to be minimized:

$$\delta E = \delta \int \left\{ \frac{4}{\pi} U \sin^2\left(2\alpha + \frac{\pi}{2}\right) \left[ \left(\frac{\pi}{4}\right)^2 + \alpha^2 \right]^{1/2} + S\alpha'^2 \right\} \mathrm{d}x = 0. \tag{59}$$

The Euler–Lagrange equation is

$$2S/U\alpha'' = (\delta/\delta\alpha)\{(4/\pi)\sin[2(2\alpha + \pi/2)][(\pi/4)^2 + \alpha^2]^{1/2}\} \tag{60}$$

with the boundary conditions $\alpha = -\pi/4$ for $x = -\infty$ and $\alpha = \pi/4$ for $x = \infty$. The solution near the corner can be found for small values of $\alpha$ in a series expansion in $\alpha$:

$$2S/U\alpha'' = -A\alpha + B\alpha^2 \ldots \qquad \text{with } A, B > 0. \tag{61}$$

In fact, numerical comparison between the full equation and this series expansion shows that for all $\alpha$-values between $-\pi/4$ and $\pi/4$ the approximation is excellent. Deviations are large outside this interval but the boundary conditions disallow such $\alpha$-values anyway. The solution for the wall trajectory is then, to a good approximation,

$$\alpha = (\pi/4)\tanh(x/\lambda) \tag{62}$$

where $\lambda \propto (S/U)^{1/2}$ is a measure for the bending radius of the wall around the corner. Note that for mesoscopic structures with a multitude of right-angled walls, such as in tartan patterns, $\lambda$ introduces again a length scale which is of the same order of magnitude as the length scale of the wall bending near defects or in needle domains if such bending is also determined by the same anisotropy energy and the bending energy. The wall trajectory in figure 11 is obtained in the $(x, y)$ coordinate system by integration:

$$y = \lambda \ln[\cosh(x/\lambda)]. \tag{63}$$

This shows the rounding of the corner.

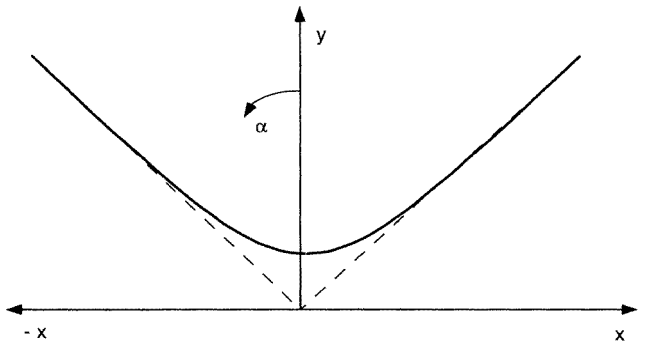


**Figure 11.** Bending of a domain wall at a right-angled corner.

## 4. Dynamical excitations and coarsening rates

The dynamical response of a ferroelastic or co-elastic material which incorporates mesoscopic twin structures may be, in a first approximation, decoupled into the bulk phonon branches, the vibrations of the domain walls and localized waves near the domain

walls. Furthermore, the domain walls can change their shape, usually while coarsening the mesoscopic structure.

Localized excitations have properties similar to those of surface waves. In experimental terms they may broaden the phonon line profiles of the twin-free material in a characteristic way. In order to derive some of their important properties we consider first the elastic excitations of the acoustic phonon branch with

$$\mathrm{d}^2u/\mathrm{d}t^2 - c^2\Delta u = 0 \tag{64}$$

and seek solutions which are constrained to the twin wall. Their amplitude may decay exponentially in the bulk of the material. With the *ansatz*

$$u_y = u_{y0}\exp[\mathrm{i}(kx - \omega t)]\exp(-y/\lambda) \tag{65}$$

we find a solution for $\lambda$ with

$$(1/\lambda)^2 = k^2 - \omega^2/c^2 \tag{66}$$

which has real values only if $k^2 > \omega^2/c^2$. The $k$ vectors of these excitations are larger than those of the equivalent bulk excitations. Waves with smaller wavevectors show no confinement nor do elastic waves. Nesting of the acoustic phonon branch, on the other hand, leads to strong localization of twin walleaves.

Mode confinement is essentially related to the fact that the twin wall is a rather softer object than the surrounding bulk material. Beyond the usual surface-type excitations, additional waves exist which are related to the relaxation of the wall itself. Their amplitude function $u_y$ has to fulfil the conditions for displacements perpendicular to the wall:

$$\sigma_{xx} = C_{12}u_{yy} \tag{67}$$

$$\sigma_{yy} = C_{11}u_{yy} \tag{68}$$

$$\sigma_{xy} = 2C_{66}u_{xy}. \tag{69}$$

The dynamical elastic response can then be written as

$$\rho\,\delta^2u_y/\delta t^2 = C_{11}\,\delta^2u_y/\delta y^2 + 2C_{66}\,\delta^2u_y/\delta x^2 \tag{70}$$

or

$$-\rho\omega^2 = C_{11}(1/\lambda)^2 - 2C_{66}k^2. \tag{71}$$

The lateral movement of the wall is determined for small amplitudes by the Peierls forces

$$\delta u_y/\delta y = -Pu_y = -(1/\lambda)u_y \tag{72}$$

which determines the length scale $\lambda$. Here we consider wall sections which are small compared with the wavelength of the vibration. For small Peierls forces the length scale of the relaxation can be larger than the actual thickness $w$ of the domain wall. The dispersion of the mode is then, for large $k$ vectors parallel to the wall,

$$(\omega/k)^2 = 2C_{66}/\rho - C_{11}/\lambda^2\rho k^2 \qquad k \gg 0. \tag{73}$$

This estimate has significant consequences for the observation of phonon dispersions in heavily twinned material. We anticipate that the wall-related excitations shift the acoustic phonon branches towards lower energies, leading to an asymmetric line broadening of the equivalent phonon spectra in neutron scattering experiments.

A similar effect is also expected for the high-frequency optical phonon branches to occur. High-frequency phonons (so-called hard modes) are often used for the characterization of structural phase transitions and show typically shifts of some 2% of their phonon frequencies due to the phase transition [43–46]. These phonon branches have small Ornstein–Zernicke

lengths, i.e. they detect the structural state on a length scale of some interatomic distances. The actual wall thickness may well exceed the Ornstein–Zernicke length so that hard modes see the strain profiles of the wall. Their profiles are then the simple superposition of the local phonon modes. Consider now the usual case that high-frequency phonons harden in the ferroelastic phase. The wall contains structural states with order parameters which are lower than those in the bulk. The wall related phonon signals show then lower energies than the bulk phonons which lead to low-frequency tails of spectral profiles in an infrared absorption or Raman scattering experiment. Note that, in highly twinned material, about 10% of the material is typically in wall-related regions of the crystal which leads to a similar asymmetry of the phonon dispersion, i.e. such effects should be easily observable in ferroelastic crystals.

The dispersion relation for the vibrating wall itself is mainly determined for small Peierls forces by the anisotropy energy. Large Peierls forces will prevent large-amplitude vibrations altogether. For a weakly pinned wall the equation of motion is

$$\delta^2 u_y/\delta y^2 = (\rho/U)(\delta^2 u_y/\delta t^2) \tag{74}$$

which is an elastic wave with the velocity $(U/\rho)^{1/2}$. The dispersion relation is linear as in case of elastic bulk waves but with drastically reduced wave velocities. The dynamical structure factor decays as $k^{-2}$ as in case of Huang scattering.

If the bending energy dominates in elastically more isotropic materials, the dispersion relation changes dramatically. The equation of motion is now

$$\delta^2 u_y/\delta y^2 = (\rho/S)(\delta^4 u_y/\delta t^4) \tag{75}$$

with a parabolic dispersion

$$\omega = S/\rho K^2. \tag{76}$$

The correlation function is that derived by Fourier transformation and has the functional form of the Ornstein–Zernicke type

$$\langle u_y(x) u_y(x')\rangle \propto (1/|x - x'|)\exp[-(x - x')/\lambda] \tag{77}$$

where $\lambda = (S/\rho)^{1/2}$ is here the Ornstein–Zernicke length along the twin wall. The structure factor for the vibrating wall decays as $k^{-4}$, i.e. with the fourth power rather than quadratically as in the case of Huang scattering.

If Peierls forces become important, the dynamical response is overdamped. In the friction limit the relaxation for large anisotropy energies is

$$\delta u_y/\delta t = (U/\rho c)(\delta^2 u_y/\delta x^2) - (P/\rho c)u_y. \tag{78}$$

The solution can be found with the *ansatz*

$$u_y = \exp\left(-\frac{Pt}{\rho c}\right)\sum_k c_k \sin(kx)\exp\left(-\frac{Uk^2 t}{\rho c}\right). \tag{79}$$

The relaxation time $\tau$ is given by the exponential term as

$$\tau = \rho c/(P + Uk^2) \tag{80}$$

and decreases with increasing wavevector. The $k$ dependence of the relaxation amplitude consists of two contributions, namely a time-independent term and a time-dependent Gaussian function. Their product shows a maximum for

$$k\tan(kz) = x\rho c/eUt. \tag{81}$$

This maximum decreases with time and becomes for small wavevectors

$$k = (\rho c/2Ut)^{1/2}. \tag{82}$$

The characteristic length of the wall movement in the friction limit increases, therefore, and the microstructure coarsens with the rate law

$$\lambda = \lambda_0 t^{-\alpha} \qquad \text{with } \alpha = 1/2. \tag{83}$$

A similar argument for a system with large bending energies leads to a rate exponent

$$\alpha = 1/4. \tag{84}$$

## 5. Conclusion

It is predicted that the trajectories of twin walls close to junctions of needle domains and, similarly, in other geometrical configurations vary substantially as a function of materials parameters. Domain walls in such regions can be planar or curved in a characteristic manner.

From the careful analysis of wall trajectories it should be possible to deduce the essential energies which determine the geometrical structure of twin walls. Experimental observations are now needed in order to verify or falsify these predictions.

## References


[1] Salje E K H 1993 *Phase Transitions in Ferroelastic and Co-elastic Crystals* (Cambridge: Cambridge University Press)
[2] Van Tendeloo G, Zandbergen H W and Amelinckx S 1987 *Solid State Commun.* **63** 389
[3] Rosova A, Boulensteix C and Vavra I 1993 *Physica* C **214** 247
[4] Nouruzi-Khoransani A, Taylor K N R and Bosi S 1989 *J. Cryst. Growth* **98** 461
[5] Salje E K H and Parlinski K 1991 *Supercond. Sci. Technol.* **4** 93
[6] Marais S, Heine V, Nex C and Salje E K H 1991 *Phys. Rev. Lett.* **66** 2480
[7] Parlinski K, Heine V and Salje E K H 1993 *J. Phys.: Condens. Matter* **5** 497
[8] Parlinski K, Salje E K H and Heine V 1993 *Acta Metall. Mater.* **41** 839
[9] Salje E K H 1992 *Phase Trans. Minerals: Phys. Chem.* **96** 1518
[10] Salje E K H 1992 *Trans. Minerals* **215** 49
[11] Marais S, Salje E K H, Heine V and Bratkovsky A M 1994 *Phase Trans.* **48** 15
[12] Salje E K H 1993 *J. Phys.: Condens. Matter* **5** 4775
[13] Bratkovsky A M, Salje E K H, Marais S C and Heine V 1994 *Phase Trans.* **48** 1
[14] Putnis A and Salje E K H 1994 *Phase Trans.* **48** 85
[15] Bratkovsky A M, Marais S C, Heine V and Salje E K H 1994 *J. Phys.: Condens. Matter* **6** 3679
[16] Tsatskis I, Vul D V A, Salje E K H and Heine V 1994 *Phase Trans.* **52** 95
[17] Bratkovsky A M, Salje E K H and Heine V 1994 *Phase Trans.* **52** 77
[18] Heine V, Bratkovsky A M and Salje E K H 1994 *Phase Trans.* **52** 85
[19] Tsatskis I, Salje E K H and Heine V 1994 *J. Phys.: Condens. Matter* **6** 11 027
[20] Vul D A, Tsatskis I and Salje E K H 1995 *Phil. Mag. Lett.* **72** 277
[21] Tsatskis I and Salje E K H 1995 *Mineralog. Mag.* **59**
[22] Basch G R and Krumhausl J A 1984 *Phys. Rev. Lett.* **53** 1069
[23] Salje E K H 1995 *Phase Trans.* **55** 37
[24] Wruck B, Salje E K H, Zhang M, Abraham T and Bismayer U 1994 *Phase Trans.* **48** 135
[25] Chrosch J and Salje E KH 1994 *Physica* C **225** 111
[26] Viehland D, Xu Z and Weug Huang 1995 *Phil. Mag.* **71** 205
[27] Ho Joug Kim, Min Su Jang, Se Young Jeong and Choe Ryoug Cho 1995 *Ferroelectrics* **157** 39
[28] Nord G L 1997 *Phase Trans.* **48** 107
[29] Dacko S, Styrkowiec R, Syslo W A and Czapla Z *Ferroelectrics* **98** 659
[30] Boulesteix C and Eyring L J *Solid State Commun.* **71** 458
[31] Hu Z W, Thomas P A and Webjorn J 1995 *J. Phys. D: Appl. Phys.* **28** 189
[32] Uesu Y, Kurimura S and Yamamoto N 1995 *Appl. Phys. Lett.* **66** 2165
[33] Mori S, Yamamoto N, Koyama Y and Uesu Y 1995 *Phys. Rev.* **51** 73
[34] Mori S, Yamamoto N, Koyama Y and Uesu Y 1995 *Phys. Rev.* **52** 6158
[35] Mashiyama H, Mizota N and Tsubouchi A 1994 *Ferroelectrics* **157** 81

[36] Tsatskis I and Salje E K H 1995 *Mineralog. Mag.* **59** 623
[37] Tsatskis I and Salje E K H 1996 *Am. Min.* at press
[38] Hayward and Salje E K H 1996 *Phys. Chem. Minerals* at press
[39] Yamamoto M, Yagi K and Honjo G 1977 *Phys. Status Solidi* **41** 523
[40] Tsai F, Khiznichenko V and J M Cowley 1992 *Ultra Microscopy* **45** 55
[41] Andrews S R and Cowley R A 1986 *J. Phys. C: Solid State Phys.* **19** 615
[42] Landau L A and Lifshitz E M 1980 *Elasticity* (Oxford: Pergamon)
[43] Salje E K H 1992 *Phase Trans.* **37** 83
[44] Bismayer U 1990 *Phase Trans.* **27** 211
[45] Salje E K H, Devarajan V, Bismayer U and Guimaraes D M C 1983 *J. Phys. C: Solid State Phys.* **165** 233
[46] Salje E K H and Yagil Y 1996 *J. Phys. Chem. Solids* at press